UDC 539.4

Effects of Sc and Zr on the Texture and Mechanical Anisotropy of High Strength Al–Zn–Mg Alloy Sheets

Y. Deng,[a,1] Z. M. Yin,[a] G. F. Xu,[a] Y. J. Wang,[b] L. Y. Lu,[b] and J. Q. Duan[b]

[a] School of Materials Science and Engineering, Central South University, Hunan, Changsha, China

[b] Northeast Light Alloy Co. Ltd, Hei Longjiang, Harbin, China

[1] csudengying@163.com

Texture, mechanical anisotropy and microstructure of aged Al–Zn–Mg, Al–Zn–Mg–0.1Sc–0.1Zr and Al–Zn–Mg–0.25Sc–0.1Zr (wt.%) alloy sheets were investigated by tensile tests and electron microscopy. Sc and Zr additions do not change the texture of homogenized and cold rolled alloys, but transfer the cube texture of the aged Al–Zn–Mg alloy into β-fiber rolling texture. With increasing Sc and Zr additions, the strength significantly increases, and mechanical anisotropy is enhanced. The strength is highest parallel to the rolling direction, whereas it is lowest at a 45° angle to the rolling direction. The higher strength is mainly due to grain boundary strengthening and precipitation strengthening caused by $Al_3Sc_xZr_{1-x}$ nano-particles. The stronger mechanical anisotropy is ascribed to the rolling texture, due to the inhibitory effect of $Al_3Sc_xZr_{1-x}$ on recrystallization. A new model was successfully established to reveal the interrelation between Sc and Zr additions, texture and yield strength anisotropy of Al–Zn–Mg sheets.

Keywords: metals, mechanical anisotropy, microstructure, tensile test, electron backscatter diffraction (EBSD), transmission electron microscopy (TEM), X-ray diffraction (XRD).

Introduction. For aerospace high-strength Al–Zn–Mg alloy to achieve suitable mechanical properties, hot or cold deformation and heat treatment are inevitable, which can give rise to the development of a characteristic texture, leading to mechanical anisotropy of the final sheet products [1, 2]. The mechanical anisotropy plays a vital role in the fracture and deformation and limits the engineering applications of alloy sheets. During engineering design, only the poorest property values of the plates can be used as a design basis, and high in-plane anisotropy increases the difficulty in forming. Therefore, it is of great importance to investigate the mechanical property of alloy plates, especially for the new alloys [3].

Compared with traditional Al–Zn–Mg alloys, new Al–Zn–Mg–Sc–Zr alloys exhibit a higher strength, excellent corrosion resistance and better weldability, which can be ascribed to the formation of extremely fine and coherent $Al_3Sc_xZr_{1-x}$ nano-particles [4–6]. However, Bate [7] and co-authors indicate that when fine particles generating Zener pinning forces on grain boundaries are present, a "brass" texture develops during deformation. Furthermore, our previous work [8] reveals that the Sc and Zr can change the recrystallization texture from cubic texture to β-fiber rolling texture and transfer the recrystallization nucleation mechanism from cubic nucleation to high stored energy nucleation during static annealing. However, there are no reports attempting to correlate Sc and Zr additions (fine $Al_3Sc_xZr_{1-x}$ particles), texture, mechanical anisotropy and microstructure in aluminum alloys, which highly limits the engineering application of new Al–Zn–Mg–Sc–Zr alloy.

In this paper, we aim to investigate the effect of Sc and Zr microalloying additions on texture, mechanical anisotropy and microstructure of Al–Zn–Mg alloy sheets and try to construct a model to reveal their interrelation mechanism.

1. **Experimental**. 2-mm thick aged Al–5.65Zn–2.0Mg, Al–5.69Zn–1.98Mg–0.1Sc–0.1Zr and Al–5.7Zn–1.98Mg–0.25Sc–0.1Zr (wt.%) alloy sheets were provided by Northeast Light Alloy Co. Ltd. The detailed thermo-mechanical history of aged sheets was reported in our previous work [9].

To evaluate the in-plane mechanical anisotropy of the T6 sheets, the tensile specimens were sectioned in different orientation angles between the tensile direction and the rolling direction in rolling surface, as shown in Fig. 1. In this study, the deviation angles were set as 0, 30, 45, 60, and 90°. The mechanical properties of all studied alloys were evaluated by room temperature tensile tests on CSS-44100 tensile tester, which were carried out at a cross-head speed of 2 mm/min, using different oriented tensile specimens with a gauge length of 60 mm and a width of 15 mm.

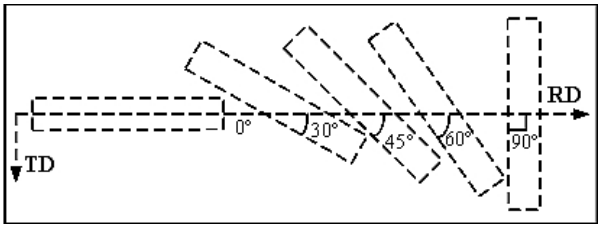

Fig. 1. The position of tensile specimens to mechanical properties.

Macrotexture measurements using standard XRD were performed on the mid-thickness rolling plane (the plane containing the rolling and transverse directions) of the specimens. EBSD analyses were performed to observe the microtexture, utilizing a Sirion 200 field emission gun scanning electron microscope equipped with EBSD system. The detailed methods for XRD and EBSD measurements were the same as our previous paper [8].

2. **Results and Discussion**.

2.1. ***Effect of Sc and Zr on In-Plane Mechanical Anisotropy of Aged Alloy Sheets***. The index of in-plane anisotropy (IPA) factor of three aged alloy sheets can be calculated according to the following equation:

$$IPA = \frac{[(N-1)X_{\max} - X_{mid1} - X_{mid2} - \ldots - X_{mid(N-2)} - X_{\min}]}{(N-1)X_{\max}} \cdot 100\%, \qquad (1)$$

where N is the number of sampling directions, $X_{\max}$ and $X_{\min}$ are the maximum and minimum values, respectively, for mechanical properties, such as elongation (EI), ultimate tensile strength (UTS), and yield strength (YS). In this study, the sectioning directions deviate from rolling direction, and the deviation angle are 0, 30, 45, 60, and 90°, and thus N is equal to 5.

Figure 2 and Table 1 show the mechanical properties of three alloys and their corresponding in-plane anisotropy indexes. As seen from Fig. 2, the strength is highest and the elongation is lowest when the tensile axis is parallel to rolling direction. Moreover, the ultimate tensile strength and yield strength of three alloys all reach their minimum values when the deviation angle is 45°. It can be found that with the increase of Sc additions the mechanical anisotropy of strength and elongation gradually increases.

T a b l e 1

IPA Values of Mechanical Properties (%)

Alloy	YS	UTS	EI
Al–Zn–Mg	1.7	1.1	6.00
Al–Zn–Mg–0.1Sc–0.1Zr	5.0	8.0	17.19
Al–Zn–Mg–0.25Sc–0.1Zr	7.2	8.2	18.08

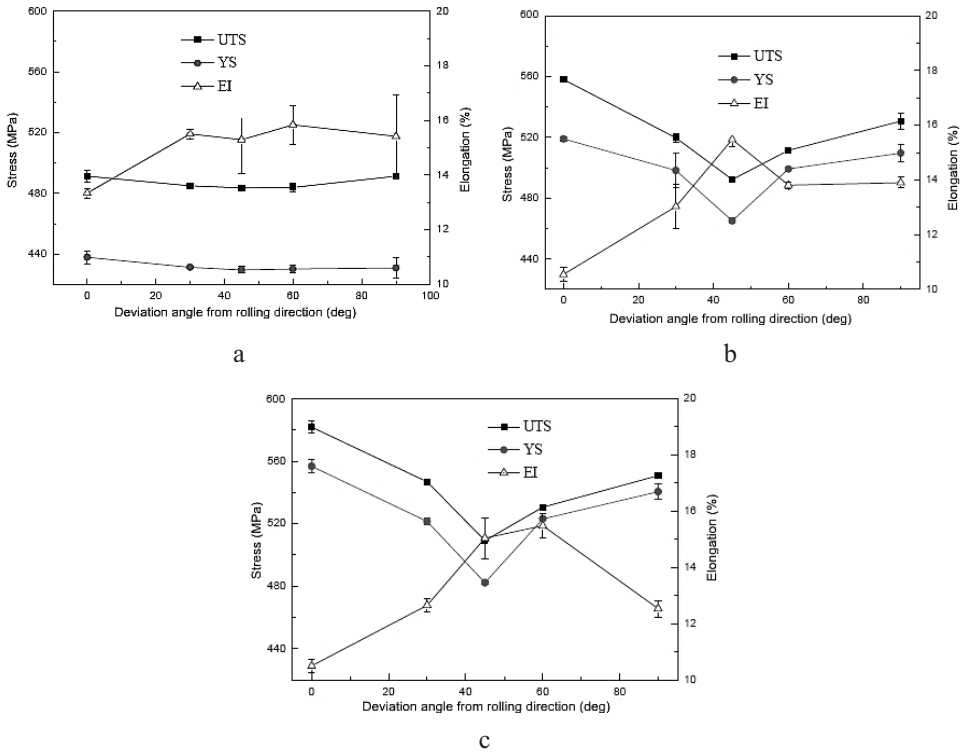

Fig. 2. Mechanical properties of three alloys stretched along different angles from rolling direction: (a) Al–Zn–Mg; (b) Al–Zn–Mg–0.1Sc–0.1Zr; (c) Al–Zn–Mg–0.25Sc–0.1Zr.

2.2. ***Macrotexture Evolution during the Preparation of Alloy Sheets***. Figure 3 shows the X-ray macrotextures of three alloys in homogenized, cold rolled and aged states. Figure 3a–c shows there is no obvious preferred orientation in homogenized alloys, except for weak {100} fiber texture. After cold rolling, β-fiber texture, containing Cu orientation {112}<111>, S orientation {123}<634>, and brass orientation {011}<112>, forms in three alloys. Besides, weak cube texture can be observed. In aged alloys, Al–Zn–Mg alloy is characterized by a strong cube texture, while it is interesting to find that two Sc-enriched alloys still retain strong rolling texture and the level of the texture density increases as compared with the cold-rolled alloys. Moreover, β-fiber rolling texture increases with the increase of Sc additions.

In order to provide more detailed quantitative texture data, the maximum intensities of orientation distribution function (ODF) $f(g)$ for a particular angle φ_1 along the α-fiber and an angle φ_2 along the β-fiber are depicted in Fig. 4. It can be seen that there is no obvious texture in homogenized alloys. The intensity of the rolling texture in two rolled and aged Sc-enriched alloys is higher than that in the Sc-free alloy. Moreover, the highest intensity of the α-fiber texture appears at the position of brass orientation, and for the β-fiber texture, it appears at the position of Cu orientation. With the increase of Sc additions, the overall β-fiber texture sharpness enhances.

2.3. ***Microstructure and Microtextures***. Figure 5 shows the EBSD microstructures and the corresponding microtextures of the three aged alloys. The color of each grain is coded by its crystal orientation based on [001] inverse pole figure as shown in Fig. 5.

As seen from Fig. 5, the microstructure of the aged Al–Zn–Mg alloy is mostly characterized by coarse recrystallized equiaxed grains with cube texture and weak S texture, and the average grain size is determined to be about 16.0 μm. However, the two

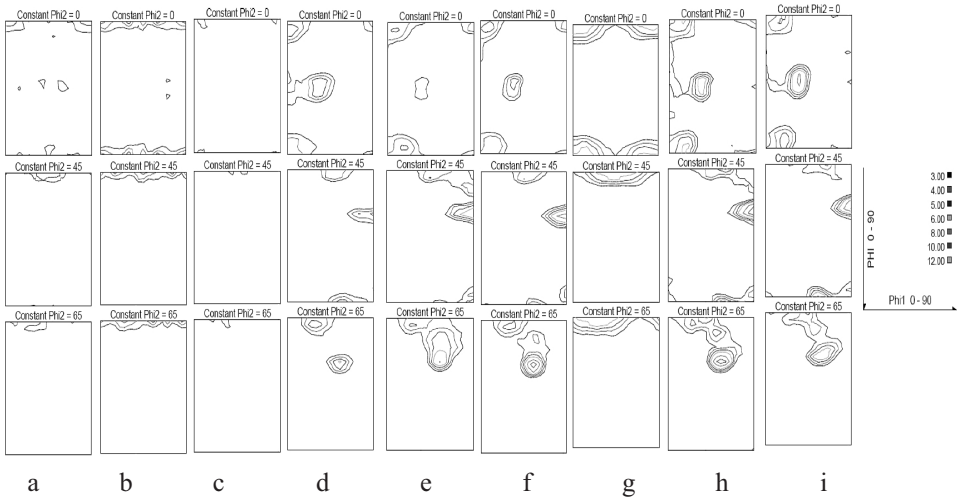

Fig. 3. ODFs representative sections of three Al–Zn–Mg alloys under typical thermomechanical conditions: Al–Zn–Mg [(a) homogenized, (d) cold rolled, (g) aged]; Al–Zn–Mg–0.1Sc–0.1Zr [(b) homogenized, (e) cold rolled, (h) aged]; Al–Zn–Mg–0.25Sc–0.1Zr [(c) homogenized, (f) cold rolled, (i) aged].

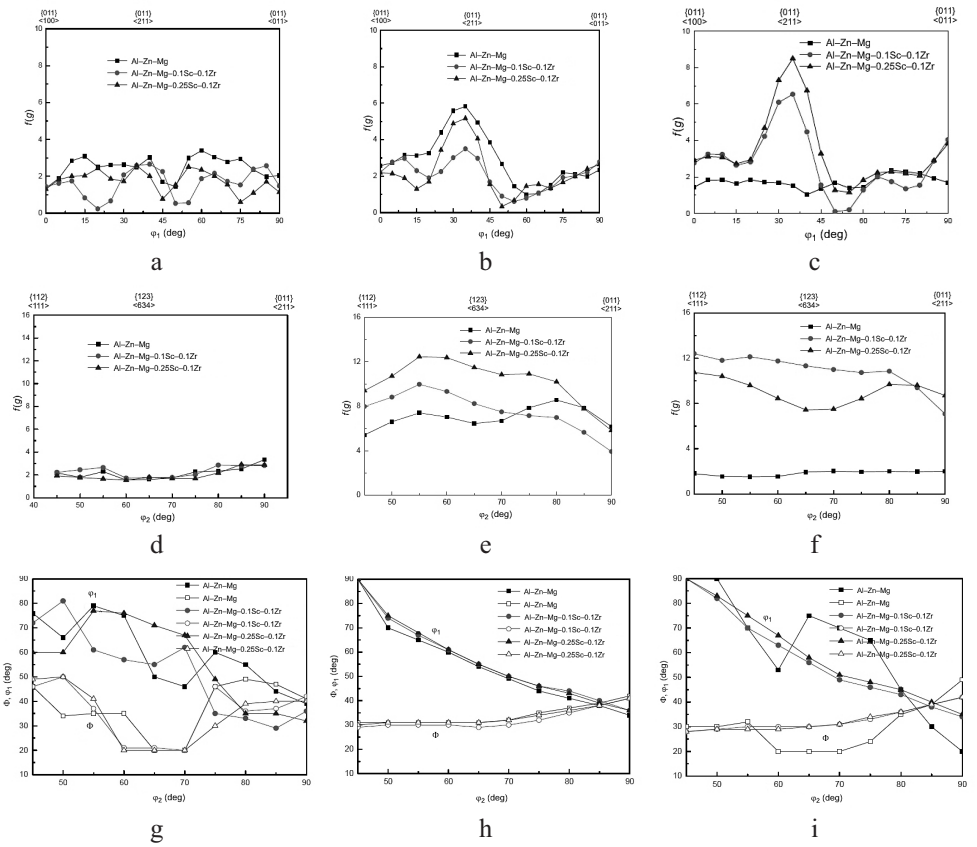

Fig. 4. Texture evolution of three alloys annealed under typical thermomechanical conditions: orientation densities $f(g)_{\max}$ along α-fiber [(a) homogenized, (b) cold rolled, (c) aged]; orientation densities $f(g)_{\max}$ along β-fiber [(d) homogenized, (e) cold rolled, (f) aged]; exact position of β-fiber in Euler space [(g) homogenized, (h) cold rolled, (i) aged].

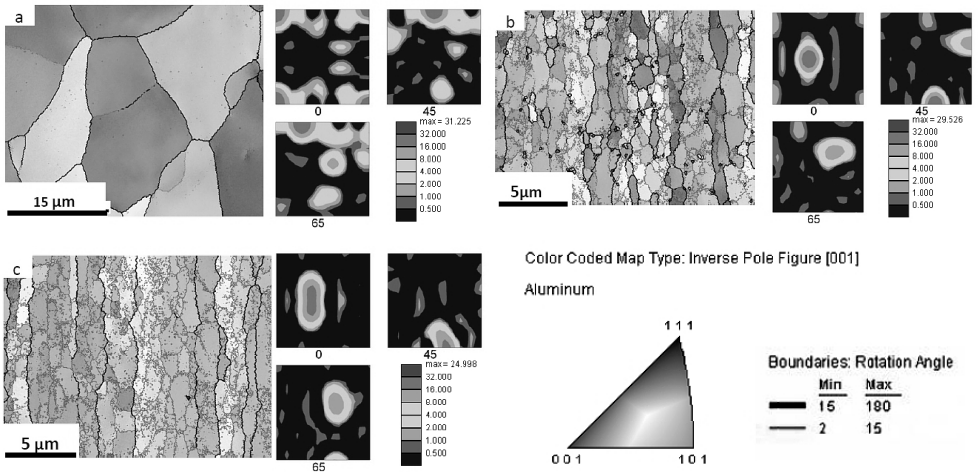

Fig. 5. EBSD images and the corresponding microtextures of three aged alloys: (a) Al–Zn–Mg; (b) Al–Zn–Mg–0.1Sc–0.1Zr; (c) Al–Zn–Mg–0.25Sc–0.1Zr.

aged Al–Zn–Mg–Sc–Zr alloys still remain un-recrystallized deformed structure, which consists of sub-grains with a high fraction of low angle grain boundaries, and have strong rolling texture. Besides, we can find that the fraction of high angle grain boundaries decrease with the increase of Sc additions, indicating that Sc additions play an important role in preventing recrystallization.

Figure 6 shows the TEM microstructures of three aged alloys. Very fine aging phases in high density were distributed in the interior of grains in three studied alloys. According to our previous work and reference [9, 10], the ageing precipitates can be identified as η' phase, which is a metastable hexagonal phase, semi-coherent with the aluminum matrix, and is the main hardening precipitate in Al–Zn–Mg alloy. Besides, in two Al–Zn–Mg–Sc–Zr alloys, secondary coherent $Al_3Sc_xZr_{1-x}$ particles in the size of about 20–40 nm, judged by their Ashby–Brown contrast for bright-field TEM images can be observed. $Al_3Sc_xZr_{1-x}$ particles can provide effective Zenner pinning force on the migration of grain boundaries and movement of dislocations. This is the main reason for the reservation of strong rolling texture in Al–Zn–Mg–Sc–Zr alloys. Moreover, with the increase of Sc additions, the density for $Al_3Sc_xZr_{1-x}$ particles increases, leading to a lower degree of un-recrystallization. Besides, except for η' phase, $Al_3Sc_xZr_{1-x}$ particles can further strengthen Al–Zn–Mg–Sc–Zr alloys, resulting in a higher strength, as shown in Fig. 2.

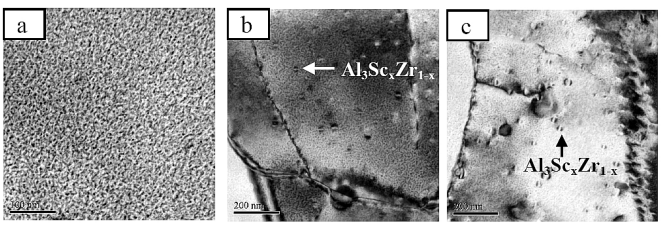

Fig. 6. TEM microstructures of the three aged alloys: (a) Al–Zn–Mg; (b) Al–Zn–Mg–0.1Sc–0.1Zr; (c) Al–Zn–Mg–0.25Sc–0.1Zr.

2.4. ***Effect of Sc and Zr on Texture during the Preparation of Al–Zn–Mg Alloy Sheets***. For most of liquid metal materials, the final products should be manufactured by solidification and crystallization processes. During the solidification, the atomic arrangement of crystallized material changes from a short-range order to a long-range order. The

solidification of metals requires two steps: in the first step, ultra-fine crystallites, known as the nuclei of a solid phase, form from the liquid. In the second step, which can overlap with the first, the ultrafine solid crystallites begin to grow as atoms from the liquid are attached to the nuclei until no liquid remains. If the nuclei in the liquid metals are formed homogeneously, the solidified structure would orientate randomly. This is why there is no obvious preferred orientation in the homogenized alloys. However, under the industry casting condition, the grains will range in the direction of heat dissipation, such as the columnar grains, and thus weak {100} fiber texture is formed, just as shown in Fig. 3. Sc and Zr additions can't change the temperature gradient generated during the casting and solidification. Therefore, they have less effect on the texture of homogenized alloys. During deformation, the grains rotate as well as elongate, causing certain crystallographic directions and planes to become aligned with the direction in which stress is applied. Consequently, after cold rolling, strong rolling textures develop. Besides, in cold rolled sheet, there is weak cube texture, whose formation can be ascribed to the recovery and recrystallization process, occurring in hot rolling and annealing before cold rolling. The recrystallization temperature for Al–Zn–Mg alloy is about 300–400℃. After solution treatment (470℃/1 h) and aging treatment, full recrystallization occurr in Al–Zn–Mg alloy, while the two Al–Zn–Mg–Sc–Zr alloys remain fiber deformed grains. Therefore, in aged alloys, the Al–Zn–Mg alloy is characterized by cube texture, and Al–Zn–Mg–Sc–Zr alloy mainly consists of rolling texture. The reservation of rolling texture in Al–Zn–Mg– Sc–Zr alloys is mainly due to the inhibitory effect of $Al_3Sc_xZr_{1-x}$ on recrystallization.

2.5. ***Effect of Sc and Zr on Mechanical Anisotropy of High Strength Al–Zn–Mg Alloy Sheets***. As seen from Table 1, with the increase of Sc and Zr additions, the mechanical anisotropy gradually increases. To explain this phenomenon, it should be related to texture and microstructures.

The deformation resistance of metals is anisotropic. According to Schmid law, the critical resolved shear stress is given by [11]:

$$\tau_c = \sigma \cos\Phi \cos\lambda, \tag{2}$$

where τ_c is critical resolved shear stress, $\cos\Phi\cos\lambda$ is Schmid factor, Φ is angle between the normal to the slip plane and the applied force, λ is the angle between the slip direction and the applied force, and σ is yield stress.

For the polycrystal materials, the yield strength can be expressed as

$$\sigma = \Delta\sigma_{gb} + M(\Delta\tau_0 + \Delta\tau_{ss} + \Delta\tau_{ppt}), \tag{3}$$

where $\Delta\tau_0$ is the critical resolved shear stress (CRSS) of pure Al (about 7 MPa), $\Delta\sigma_{gb}$, $\Delta\tau_{ss}$, and $\Delta\tau_{ppt}$ are the strengthening contribution from subgrain boundaries, solid solution, and precipitation, respectively, and M is Taylor factor, depending on textures and orientation of tensile axis. As seen from Eq. (2), to calculate the yield stress under different tensile direction, it should determine M values. Several models have been proposed to calculate the M factor of a material at a giving orientation, such as the Sachs model [12], the Hutchinson model [13], and the Taylor model [14]. However, in our case, the aged sheet, especially Al–Zn–Mg–Sc–Zr alloys, contains several grain orientations, and based on authors' knowledge, no model is available to determine which slip systems will be activated in each grain for such a case.

In this paper, a new model is proposed with the assumption that all the slip systems may, with varying probabilities, contribute to plastic deformation, and the slip system with higher Schmid factor value has a higher chance of being activated. This model can be expressed as

$$M(\alpha)^{-1} = \sum_{i=1}^{n} f_i \sum_{j=1}^{12} w_j m_{i,j}(\alpha) + f_{random} m, \tag{4}$$

where $M(\alpha)$ is the M factor when the angle between the tensile axis and rolling direction is α, f_i is the volume fraction of i texture component, f_{random} is the fraction of randomly orientated grains, m is the Schmid factor for random texture (about 0.33). FCC Al alloys contain four {111} slip planes and three <111> (slip directions) within each plane, giving 12 slip systems, and $m_{i,j}(\alpha)$ is the Schmid factor in the order of j when the angle between the tensile direction and rolling direction is α. The magnitude of $m_{i,j}(\alpha)$ is in the order $m_{i,1}(\alpha) > m_{i,2}(\alpha) > \ldots > m_{i,j}(\alpha) > \ldots > m_{i,12}(\alpha)$, where $i \geq 4$, $j \geq 12$. w_j is the weight coefficient for each $m_{i,j}(\alpha)$, and satisfies the following condition:

$$\sum_{j=1}^{12} w_j = 1, \tag{5}$$

$$\frac{w_j}{w_{j+1}} = \left(\frac{m_{i,j}}{m_{i,j+1}} \right)^n, \tag{6}$$

where n a positive integer, $n \geq 4$. During the calculation, we assume that all slip system participate in slipping, and the higher Schmid factor, the more opportunity to participate in slipping.

The standard Hall–Petch equation was employed to relate the yield strength of the material (σ) to the average grain size (d),

$$\sigma_{H-P} = \sigma_0 + kd^{-1/2}. \tag{7}$$

In this equation, σ_0 is the intrinsic resistance of the lattice to dislocation motion and k is a parameter that describes the relative strengthening contribution of grain boundaries. A k value of 0.04 MPa $\cdot$ m$^{1/2}$ for aluminum was used to estimate the strengthening due to grain boundaries.

By substituting of k value and grain sizes in three studied alloys obtained from EBSD, $\Delta\sigma_{gb}$, the increase in the YS due to the grain boundary strengthening, were 14, 34, and 42 MPa in Al–Zn–Mg, Al–Zn–Mg–0.1Sc–0.1Zr, and Al–Zn–Mg–0.25Sc–0.1Zr, respectively.

For peak aged alloys, η' is the aging strengthening phase for Al–Zn–Mg alloy, and in Al–Zn–Mg–Sc–Zr alloys, there exist two precipitates: η' and $Al_3Sc_xZr_{1-x}$ particles. Value of τ_{ppt} can be calculated as

$$\tau_{ppt} = \frac{2\beta Gb}{r} \sqrt{\frac{3f}{2\pi}}, \tag{8}$$

where β is constant, about 0.36, r is the radius of precipitate (in this study, according to the TEM images, the sizes of η' and $Al_3Sc_xZr_{1-x}$ were determined to be 12 and 20 nm, respectively), and f is the volume fraction of precipitates. As there is some difference in the weight fractions of Zn and Mg among the three alloys, the volume fractions of aging precipitate are calculated to be 4.19, 3.84, and 4.22% in Al–Zn–Mg, Al–Zn–Mg–0.1Sc–0.1Zr, and Al–Zn–Mg–0.25Sc–0.1Zr alloys by using JMatPro 5.1 thermodynamic software,

respectively. Moreover, the volume fractions for $Al_3Sc_xZr_{1-x}$ particles are 0.35 and 0.71% in Al–Zn–Mg–0.1Sc–0.1Zr and Al–Zn–Mg–0.25Sc–0.1Zr alloys, respectively. Therefore,

$\Delta\tau_{ppt} = \Delta\tau_{ppt-MgZn_2} = 135$ MPa (Al–Zn–Mg alloy),

$\Delta\tau_{ppt} = \Delta\tau_{ppt-MgZn_2} + \Delta\tau_{ppt-Al_3(Sc,Zr)} = 129+23 = 152$ MPa (Al–Zn–Mg–0.1Sc–0.1Zr alloy),

$\Delta\tau_{ppt} = \Delta\tau_{ppt-MgZn_2} + \Delta\tau_{ppt-Al_3(Sc,Zr)} = 135+33 = 168$ MPa (Al–Zn–Mg–0.25Sc–0.1Zr alloy).

Value of $\Delta\tau_{ss}$ can be calculated as

$$\Delta\tau_{ss} = KC^{2/3}, \tag{9}$$

where K is a constant and C is the average concentration of solute atoms. Combined with the JMatPro calculation results (the concentrations for solute atoms are about 7.2 wt.% in solution state and 0.6 wt.% in aged state), $\Delta\tau_{ss}$ are determined to be 10, 9, and 8 MPa in Al–Zn–Mg, Al–Zn–Mg–0.1Sc–0.1Zr, and Al–Zn–Mg–0.25Sc–0.1Zr alloys, respectively.

In conclusion, the yield strength for three aged alloys can be calculated by the following equations:

$$\text{Al–Zn–Mg:}\ \ \sigma = 14+152M, \tag{10}$$

$$\text{Al–Zn–Mg–0.1Sc–0.1Zr:}\ \ \sigma = 34+168M, \tag{11}$$

$$\text{Al–Zn–Mg–0.25Sc–0.1Zr:}\ \ \sigma = 42+183M. \tag{12}$$

Table 2 shows the volume fractions of different texture components in three aged alloys. It can be found that with the increase of the content of Sc additions the volume fractions of rolling textures, including S, brass, and Cu orientations, increase, while the cube and random textures weaken. For the Al–Zn–Mg–0.25Sc–0.1Zr aged sheet, it is mainly composed of rolling texture components. Table 3 shows the calculated Taylor factors under different tensile directions.

Table 2

Volume Fractions of Different Texture Components (Combined with the Results from XRD and EBSD)

Alloy	Cu	S	Brass	Cube	Random
Al–Zn–Mg	0.018	0.224	0.011	0.275	0.472
Al–Zn–Mg–0.1Sc–0.1Zr	0.175	0.349	0.385	0.022	0.069
Al–Zn–Mg–0.25Sc–0.1Zr	0.200	0.380	0.400	0.000	0.020

By substituting the above data into Eqs. (10)–(12), the calculated yield strength under different angles between tensile direction and rolling direction are shown in Fig. 7. As seen from Fig. 7, it can be found that the established model can well reflect the internal law between the yield stress, tensile orientations and texture. Besides, the calculated data are closer to the experimental data, when n is 4–5 in Al–Zn–Mg alloy, n is 5–6 in Al–Zn–Mg–0.1Sc–0.1Zr alloy, and n is 6–∞ in Al–Zn–Mg–0.25Sc–0.1Zr alloy, respectively; n increases with the increase of Sc and Zr contents. This can be inferred that with the increase of Sc and Zr additions, only the slipping systems with the higher Schimd factors have the opportunity to overcome the Zenner pinning of $Al_3Sc_xZr_{1-x}$ particles to participate in plastic deformation.

T a b l e 3

Values of *M* under Different Tensile Directions

Alloy	0	30°	45°	60°	90°
$n = 4$					
Al–Zn–Mg	2.803	2.762	2.742	2.767	2.747
Al–Zn–Mg–0.1Sc–0.1Zr	2.879	2.851	2.577	2.885	2.910
Al–Zn–Mg–0.25Sc–0.1Zr	2.891	2.850	2.557	2.890	2.898
$n = 5$					
Al–Zn–Mg	2.781	2.710	2.716	2.716	2.724
Al–Zn–Mg–0.1Sc–0.1Zr	2.810	2.779	2.469	2.812	2.871
Al–Zn–Mg–0.25Sc–0.1Zr	2.817	2.774	2.440	2.815	2.856
$n = 6$					
Al–Zn–Mg	2.764	2.681	2.703	2.687	2.709
Al–Zn–Mg–0.1Sc–0.1Zr	2.759	2.730	2.424	2.764	2.844
Al–Zn–Mg–0.25Sc–0.1Zr	2.762	2.724	2.392	2.764	2.827
$n = +\infty$					
Al–Zn–Mg	2.700	2.600	2.500	2.677	2.656
Al–Zn–Mg–0.1Sc–0.1Zr	2.608	2.554	2.298	2.604	2.755
Al–Zn–Mg–0.25Sc–0.1Zr	2.601	2.538	2.272	2.588	2.732

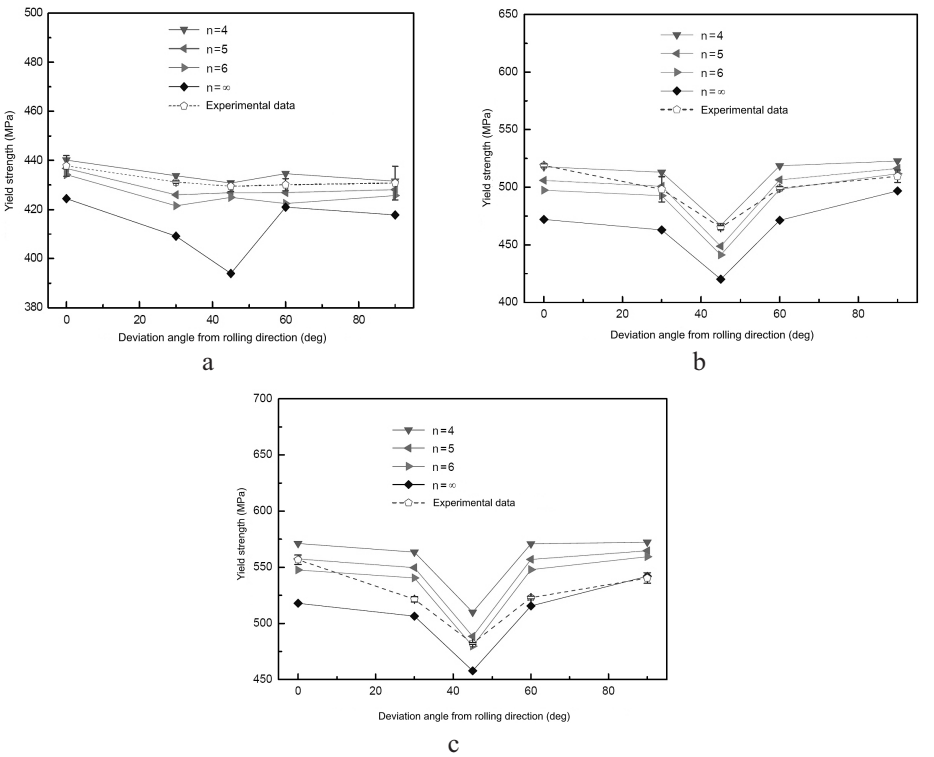

Fig. 7. The caluculated yield stress values and experimental data under different tensile directions: (a) Al–Zn–Mg; (b) Al–Zn–Mg–0.1Sc–0.1Zr; (c) Al–Zn–Mg–0.25Sc–0.1Zr.

The Schmid factors of different slipping systems are determined by the textures. The Al–Zn–Mg–Sc–Zr alloy consists of strong rolling texture components, whose M values are smaller in case of a 45° angle between rolling direction and tensile direction, and thus the yield strength value is the lowest under this tensile condition. Moreover, with the increase of Sc and Zr additions, the volume fractions of S, brass, and Cu orientations increase, while random texture decreases correspondingly, and thus the mechanical anisotropy enhances.

Conclusions. Texture, mechanical property and microstructure of high strength Al–Zn–Mg, Al–Zn–Mg–0.1Sc–0.1Zr, and Al–Zn–Mg–0.25Sc–0.1Zr alloys were investigated by XRD diffraction measurement, tensile tests, transmission electron microscopy and electron back scattered diffraction methods. The following conclusions can be drawn from this study.

1. The three homogenized alloys mainly consist of random texture. In cold rolled alloys, cube orientation and rolling texture are dominant. After solution-aging treatment, full recrystallization occurs in Al–Zn–Mg alloy and the texture transfers into cube texture. However, un-recrystallized deformed structures remain in two Al–Zn–Mg–Sc–Zr alloys, and the alloys have strong β-fiber rolling texture.

2. For aged alloys, the ultimate tensile strength and yield strength increase with increasing the Sc and Zr additions, meantime, the mechanical anisotropy enhances.

3. To explain the yield strength anisotropy, a new model is established, which can well reflect the internal law between the yield stress, tensile orientations and texture. It can be inferred that the preferred orientation is the main factor to mechanical anisotropy. The higher mechanical anisotropy can be ascribed to the strong β-fiber rolling texture, caused by the inhibitory effect of nano-scaled $Al_3Sc_xZr_{1-x}$ particles on recrystallization during the preparation of aged sheets.

Acknowledgments. The authors gratefully acknowledge the financial support from the National General Pre-research Project of China (51312010402) and the China Postdoctoral Science Foundation (2014M552149).

1. N. P. Gurao, A. O. Adesola, A. G. Odeshi, and J. A. Szpunar, “On the evolution of heterogeneous microstructure and microtexture in impacted aluminum–lithium alloy,” *J. Alloys Compd*., **578**, 183–187 (2013).
2. J. R. Hirsch and T. Al-Samman, “Superior light metals by texture engineering: Optimized aluminum and magnesium alloys for automotive applications,” *Acta Mater.*, **61**, 818–843 (2013).
3. C. Booth-Morrison, D. C. Dunand, D. N. Seidman, “Coarsening resistance at 400℃ of precipitation-strengthened Al–Zr–Sc–Er alloys,” *Acta Mater.*, **59**, 7029–7042 (2011).
4. A. K. Mukhopadhyay, A. Kumar, S. Raveendra, and I. Samajdar, “Development of grain structure during superplastic deformation of an Al–Zn–Mg–Cu–Zr alloy containing Sc,” *Scripta Mater.*, **64**, 386–389 (2011).
5. M. E. van Dalen, T. Gyger, D. C. Dunand, and D. N. Seidman, “Effects of Yb and Zr microalloying additions on the microstructure and mechanical properties of dilute Al–Sc alloys,” *Acta Mater.*, **59**, 7615–7626 (2011).
6. K. E. Knipling, D. N. Seidman, and D. C. Dunand, “Ambient- and high-temperature mechanical properties of isochronally aged Al–0.06Sc, Al–0.06Zr and Al–0.06Sc–0.06Zr (at.%) alloys,” *Acta Mater.*, **59**, 943–954 (2011).
7. P. S. Bate, Y. Huang, and F. J. Humphreys, “Development of the “brass” texture component during the hot deformation of Al–6Cu–0.4Zr,” *Acta Mater.*, **52**, 4281–4289 (2004).

8. Y. Deng, G. F. Xu, Z. M. Yin, et al., "Effects of Sc and Zr microalloying additions on the recrystallization texture and mechanism of Al–Zn–Mg alloys," *J. Alloys Compd*., **580**, 412–426 (2013).
9. Y. Deng, Z. M. Yin, J. Q. Duan, et al., "Evolution of microstructure and properties in a new type 2 mm Al–Zn–Mg–Sc–Zr alloy sheet," *J. Alloys Compd.*, **517**, 118–126 (2012).
10. Y. Deng, Z. M. Yin, K. Zhao, et al., "Effects of Sc and Zr microalloying additions on the microstructure and mechanical properties of new Al–Zn–Mg alloys," *J. Alloys Compd.*, **530**, 71–80 (2012).
11. D. R. Askeland and P. P. Phulé, *Essentials of Materials Science and Engineering*, 1st edn, Ch. 4: *Imperfections in the Atomic and Ionic Arrangements*, Thomson Learning (2004), pp. 99–101.
12. L. M. Brown and R. K. Ham, *Strengthening Methods in Crystals*, Elsevier, Amsterdam (1971).
13. J. W. Hutchinson, "Elastic-plastic behaviour of polycrystalline metals and composites," *Proc. Roy. Soc. London A*, **319**, 247–272 (1970).
14. M. J. Starink and S. C. Wang, "A model for the yield strength of overaged Al–Zn–Mg–Cu alloys," *Acta Mater.*, **51**, 5131–5150 (2003).

Received 03.08. 2015